

Nonrealizable Planar and Spherical Occlusion Diagrams

Kimberly Kokado¹ and Csaba D. Tóth¹

California State University Northridge, Los Angeles, CA, USA
kimberly.kokado.43@my.csun.edu, csaba.toth@csun.edu

Abstract. Spherical occlusion diagrams (SOD) were introduced by Viglietta as an axiomatic framework to analyze the visibility maps of points in the interior of a nonconvex polyhedron from which no vertex is visible; and conjectured that every SOD is realizable as a visibility map of a point in some polyhedron. In this paper, we disprove this conjecture, and construct an SOD that is not realizable as a visibility map.

Keywords: spherical occlusion diagram, visibility map, realization space

1 Introduction

The classical *art gallery problem* asks for the minimum number of point guards that can jointly see all points in a nonconvex polyhedron \mathcal{P} in Euclidean space, where points s and t see each other if the line segment st is contained in \mathcal{P} . It is well known that guards stationed at the vertices of \mathcal{P} do not always suffice in \mathbb{R}^3 , as some points $s \in \mathbb{R}^3$ in the interior of a polyhedron \mathcal{P} may not see any of the vertices [5, Sec. 10.2]. Viglietta [9, 10] recently introduced *spherical occlusion diagrams* (SOD, for short) to analyze the visibility map $V_{\mathcal{P}}(s)$ of such a point s with respect to \mathcal{P} . An SOD is defined (cf. Section 2) so that it satisfies key properties of visibility maps. In particular, if no vertices of a polyhedron \mathcal{P} are visible from a viewpoint s , then the visibility map $V_{\mathcal{P}}(s)$ is an SOD. Initially, Viglietta [9, version 1] conjectured that the converse also holds; that is, every SOD is the visibility map $V_{\mathcal{P}}(s)$ for some point s and polyhedron \mathcal{P} in \mathbb{R}^3 . The main result of this paper (Theorem 2) disproves this conjecture by constructing an SOD that is not realizable as a visibility map in \mathbb{R}^3 . In subsequent versions of Viglietta's paper [10], this conjecture was replaced with a reference to our counterexample. More recently, Viglietta [10, Conjecture 5] conjectured that the counterexample can be strengthened and there exists an *irreducible* SOD (defined below) that is not realizable. We prove this recent conjecture and construct an irreducible SOD that is not realizable (Theorem 3).

Related work. Our results show that SODs are not always visibility maps. Nevertheless, SODs have already been used in 3-dimensional visibility problems: Cano et al. [2] proved that every polyhedron \mathcal{P} in \mathbb{R}^3 can be guarded by at most $\frac{5}{6}$ of its edges; moreover, when \mathcal{P} is homeomorphic to a ball and all its faces are

triangles, it can be guarded by at most $\frac{29}{36}$ of its edges. Tóth et al. [8] proved that every point that does not see any vertex of a polyhedron \mathcal{P} must see at least 8 edges of \mathcal{P} , and this bound is tight.

The realizability of visibility maps have been previously studied for lines. A *weaving pattern* is a simple arrangement of n lines in \mathbb{R}^2 together with a binary relation between intersecting lines; a weaving pattern is *realizable* if it is the orthogonal projection of an arrangement of disjoint lines in \mathbb{R}^3 such that the above-below relation between lines matches the given binary relation between their orthogonal projections. Pach et al. [7] showed that almost all weaving patterns of n lines are nonrealizable for sufficiently large n . Basu et al. [1] generalized the result to arrangements of semialgebraic curves.

Organization. In Section 2, we review spherical occlusion diagrams (SODs), and introduce their planar analogues, planar occlusion diagrams (PODs). In Section 3, we construct a family of PODs by modifying a well-known nonregular triangulation (depicted in Fig. 2) in four stages. In Section 4, we show that these PODs cannot be realized as visibility maps from the viewpoint $z = -\infty$. Then in Section 5, we lift the nonrealizable PODs to the sphere, using spherical projections, to obtain nonrealizable SODs. We conclude with open problems in Section 6.

2 Preliminaries

Visibility maps. We consider visibility with respect to polygonal obstacles in \mathbb{R}^3 , this setting includes visibility in a polyhedron as a special case [6]. A *polygonal scene* \mathcal{P} is a finite collection of 2-dimensional polygons in \mathbb{R}^3 with pairwise disjoint relative interiors, where a *2-dimensional polygon* is a connected set with piecewise linear boundary in an affine plane in \mathbb{R}^3 (e.g., a polygon in \mathcal{P} may be a halfplane or an unbounded 2-dimensional polytope). In particular, the collection of 2-faces of a polyhedron in \mathbb{R}^3 is a polygonal scene. Two points $s, t \in \mathbb{R}^3$ *see* each other (with respect to \mathcal{P}) if the relative interior of the line segment st is disjoint from all polygons in \mathcal{P} . For a point $s \in \mathbb{R}^3$ and a polygonal scene \mathcal{P} , the *visibility polyhedron* $V_{\mathcal{P}}(s)$ is the closure of the set of points in \mathbb{R}^3 that are visible to s (note that $V_{\mathcal{P}}(s)$ may be unbounded); and the *visibility map* \mathcal{P}_s is the projection of the vertices, edges, and faces of $V_{\mathcal{P}}(s)$ to a sphere centered at s . In particular, \mathcal{P}_s is a finite collection of geodesic arcs on a sphere, where each arc is the projection of a maximal visible line segment along an edge of a polygon in \mathcal{P} .

Instead of viewpoints $s \in \mathbb{R}^3$ and projections to a sphere, we will also work with the viewpoint at $z = -\infty$, and orthogonal projections to the xy -plane. Formally, let $V_{\mathcal{P}}(-\infty)$ be the closure of the set of points $t \in \mathbb{R}^3$ such that the relative interior of the vertical downward ray emanating from t is disjoint from all polygons in \mathcal{P} ; and let $\mathcal{P}_{-\infty}$ be the orthogonal projection of $V_{\mathcal{P}}(-\infty)$ onto the xy -plane. Equivalently, $\mathcal{P}_{-\infty}$ is the orthogonal projection of the lower envelope of \mathcal{P} to the xy -plane.

Occlusion diagrams. Let a and b be two Jordan arcs in the plane or on a sphere. If an endpoint p of a lies in the relative interior of b , we say that a *hits* b at p ; and b *blocks* a at p . Viglietta defined spherical occlusion diagrams as follows.

Definition 1 (Viglietta [10]). A *spherical occlusion diagram* (for short, *SOD*) is a finite nonempty collection \mathcal{D} of geodesic arcs on the unit sphere \mathbb{S}^2 that satisfy the following axioms:

- (1) Any two arcs in \mathcal{D} are internally disjoint.
- (2) Each arc in \mathcal{D} is blocked by arcs of \mathcal{D} at each endpoint.
- (3) All arcs in \mathcal{D} that hit the same arc of \mathcal{D} reach it from the same side.

An SOD \mathcal{D} is *irreducible* if it has no proper subset that is also an SOD. A *swirl* in an SOD is a cycle of arcs, each of which hits the next, going either all clockwise or all counterclockwise. Viglietta [10] proved that every SOD has at least four convex faces bounded by swirls.

We define planar occlusion diagrams for a collection of line segments and rays in the plane that abide axioms analogous to Definition 1.

Definition 2. A *planar occlusion diagram* (for short, *POD*) is a finite collection \mathcal{S} of line segments and rays (for short, *segments*) in the plane that satisfy the following axioms:

- (1) Any two segments in \mathcal{S} are internally disjoint.
- (2) Each segment in \mathcal{S} is blocked by segments of \mathcal{S} at each endpoint.
- (3) All segments in \mathcal{S} that hit the same segment in \mathcal{S} reach it from the same side.

A POD \mathcal{S} is *irreducible* if it has no proper subset that is also an POD. A *swirl* in a POD \mathcal{S} is a cycle of segments where each hits the next.

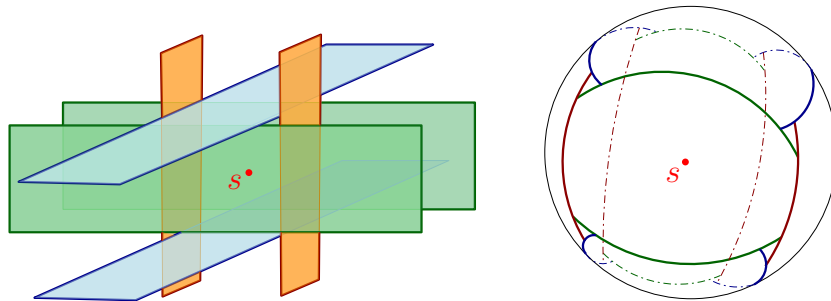


Fig. 1: Left: A polygonal scene \mathcal{P} of six pairwise disjoint axis-aligned rectangles and a viewpoint s that cannot see any vertex. Right: The visibility map \mathcal{P}_s on a unit sphere centered at s is an SOD.

Realizations. Viglietta [10, Proposition 3] showed that for every polyhedron \mathcal{P} , if a viewpoint $s \in \mathbb{R}^3$ cannot see any vertices of \mathcal{P} is not on the boundary of \mathcal{P} , then the visibility map \mathcal{P}_s is an SOD. The same argument generalizes to polygonal scenes; see Fig. 1 for an example. A *realization* of an SOD \mathcal{D} is a polygonal scene \mathcal{P} with a viewpoint s such that $\mathcal{D} = \mathcal{P}_s$. An SOD \mathcal{D} is *realizable* if it admits a realization.

Similarly, it is easily verified that if the lower envelope of a polygonal scene \mathcal{P} does not contain any vertex of \mathcal{P} , then $\mathcal{P}_{-\infty}$ is a POD. A *realization* of a POD \mathcal{S} is a polygonal scene \mathcal{P} such that $\mathcal{S} = \mathcal{P}_{-\infty}$, and \mathcal{S} is *realizable* if it admits a realization. (Note that a realization of a POD requires unbounded polygons.)

We frequently use the following easy observation. It allows us to assume that any particular nonvertical polygon in a polygonal scene is in fact horizontal.

Lemma 1. *Let \mathcal{P} be a polygonal scene in \mathbb{R}^3 , where $f \in \mathcal{P}$ is a nonvertical polygon. Then, there exists a nondegenerate affine transformation $A : \mathbb{R}^3 \rightarrow \mathbb{R}^3$ such that $A(f)$ lies in the xy -plane and $A(\mathcal{P})_{-\infty} = \mathcal{P}_{-\infty}$.*

Proof. Suppose that f lies in the plane $\text{span}(f) = \{(x, y, z) \in \mathbb{R}^3 : z = \alpha x + \beta y\}$. Then the affine transformation $A : \mathbb{R}^3 \rightarrow \mathbb{R}^3$, $A(x, y, z) = (x, y, z - (\alpha x + \beta y))$ maps $\text{span}(f)$ to the xy -plane. Since A preserves the x - and y -coordinates, as well as the above-below relationship with respect to the z -coordinate, it does not change the orthogonal projection of the lower envelope, consequently $A(\mathcal{P})_{-\infty} = \mathcal{P}_{-\infty}$, as required. \square

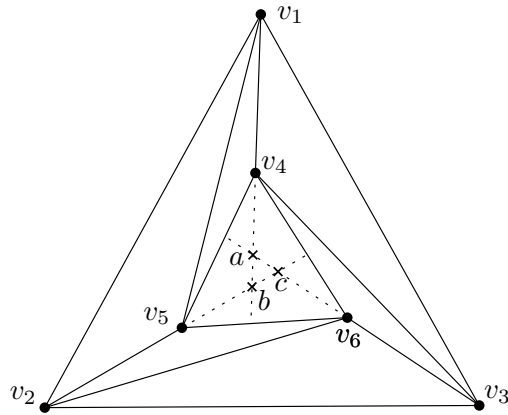


Fig. 2: A nonregular triangulation T . The triangles $\Delta v_1 v_2 v_3$, $\Delta v_4 v_5 v_6$ and Δabc are equilateral with a common barycenter. In particular, $|v_1 v_4| = |v_2 v_5| = |v_3 v_6|$.

Regular triangulations. A planar line graph is said to be *regular* if it is the orthogonal projection of the lower envelope of a convex polyhedron in \mathbb{R}^3 [4]. The

triangulation T shown in Fig. 2 is known to be nonregular [3, Example 5.1.4]. Our construction modifies the triangulation T to obtain a POD \mathcal{S} (in Section 3). We show that in any realization of \mathcal{S} , any two polygons corresponding to adjacent triangles in T have a dihedral angle at most π (Section 4). However, if the dihedral angle of two adjacent triangles in \mathbb{R}^3 equals π , then they are in fact coplanar, i.e., they are part of the same face of the convex polyhedron. The following lemma shows that T remains nonregular even if we merge some (but not all) of its faces.

Lemma 2. *There exists no convex polyhedron \mathcal{P} such that (i) the lower envelope of \mathcal{P} has two or more facets; and (ii) the triangulation T depicted in Fig. 2 is a triangulation of the orthogonal projection of the lower envelope of \mathcal{P} .*

Proof. Suppose, by contradiction, that such a convex polyhedron \mathcal{P} exists. Assume that $\mathcal{P} = \text{conv}\{\hat{v}_1, \dots, \hat{v}_6\}$, where $v_i \in \mathbb{R}^2$ is the orthogonal projection of $\hat{v}_i \in \mathbb{R}^3$ for $i = 1, \dots, 6$. We may assume, by Lemma 1, that the facet of the lower envelope of \mathcal{P} that contains $\Delta\hat{v}_4\hat{v}_5\hat{v}_6$ lies in the xy -plane. As the facets of the lower envelope of \mathcal{P} are not coplanar, then \hat{v}_1, \hat{v}_2 or \hat{v}_3 is strictly above the xy -plane.

Assume w.l.o.g. that vertex \hat{v}_1 of \mathcal{P} has the highest z -coordinate. Denote by H the plane spanned by $\Delta\hat{v}_1\hat{v}_5\hat{v}_4$. Since the dihedral angle between $\Delta\hat{v}_1\hat{v}_2\hat{v}_5$ and $\Delta\hat{v}_1\hat{v}_5\hat{v}_4$ is at most π , then \hat{v}_2 lies on or above H . If $\hat{v}_2 \in H$, then the lines $\hat{v}_1\hat{v}_4$ and $\hat{v}_2\hat{v}_4$ meet at a point $\hat{b} \in H$ that projects to b in the xy -plane (Fig. 2). However, $|bv_5| < |bv_4|$ implies that $\text{slope}(\hat{b}\hat{v}_2) > \text{slope}(\hat{b}\hat{v}_4)$, and this holds even if \hat{v}_2 lies above H . Combined with the fact that $|v_1v_4| = |v_2v_5|$, this further implies that $z(\hat{v}_2) > z(\hat{v}_1)$, contradicting our assumption that vertex \hat{v}_1 has the highest z -coordinate. This completes the proof. \square

3 Construction of Planar Occlusion Diagrams

In this section, for every sufficiently small $\varepsilon > 0$, we construct a POD \mathcal{S} . We start with the triangulation T in Fig. 2 and modify it in four stages.

Overview. Our construction proceeds in four stages. Each triangular face Δ of T will correspond to a convex face Δ' of \mathcal{S} that lies in the interior of Δ such that the boundary of Δ' is within an ε -neighborhood of Δ . The crux of the construction is to create new convex faces in the ε -neighborhood of edges and vertices of T . We enclose each vertex of T with a circle of radius ε in Stage 1, and then enclose each edges of T with a nonconvex region bounded by circular and parabolic arcs in Stage 2. We replace these regions with convex polygons in Stage 3. Finally, we perturb the convex tiling into a POD, while creating small swirls around its vertices.

In all stages of the construction of \mathcal{S} , we use auxiliary points, called *guide points*, which will not be part of the diagram \mathcal{S} . Overall, there are four types of guide points: S_1, G_1 , and S_2 *guide points* created Stage 1, respectively; and S_3 *guide points* created in Stage 3.

Stage 1. We start with the triangulation T depicted in Fig. 2 with vertices v_1, \dots, v_6 . Draw a circle of radius $\varepsilon > 0$ centered at each vertex of T . The radius $\varepsilon > 0$ must be sufficiently small so that the circles are pairwise disjoint and, for all $i = 1, \dots, 6$, a circle centered at v_i does not intersect any triangle in T that is not incident to v_i ; see Fig. 3.

We place an initial set of points, called S_1 and G_1 *guide points*, respectively, as follows. Let $\eta \in (0, \frac{\varepsilon}{2})$ be sufficiently small, to be specified later.

For each vertex v of T and each edge e of T incident to v , place two S_1 guide points on the circle centered at v at distance η from e (one on each side of e). For every edge e of T , place two G_1 guide points on the orthogonal bisector of e at distance $\eta/2$ from e (one on each side of e). The value of $\eta > 0$ should be sufficiently small such that (1) every S_1 guide point at distance η from an edge e lies in a face of T incident to e , and (2) for any two adjacent edges, e_1 and e_2 , the angle bisector of $\angle(e_1, e_2)$ separates the guide points associated with e_1 and e_2 , respectively. We shall impose a third condition on η in Stage 2.

Lastly, we place three additional guide points in the outer face, which will help extend the construction to the entire plane. For each vertex v of the outer face of T , place a guide point at the intersection of the circle centered at v and the angle bisectors of the outer face; we call these three points S_2 *guide points*.

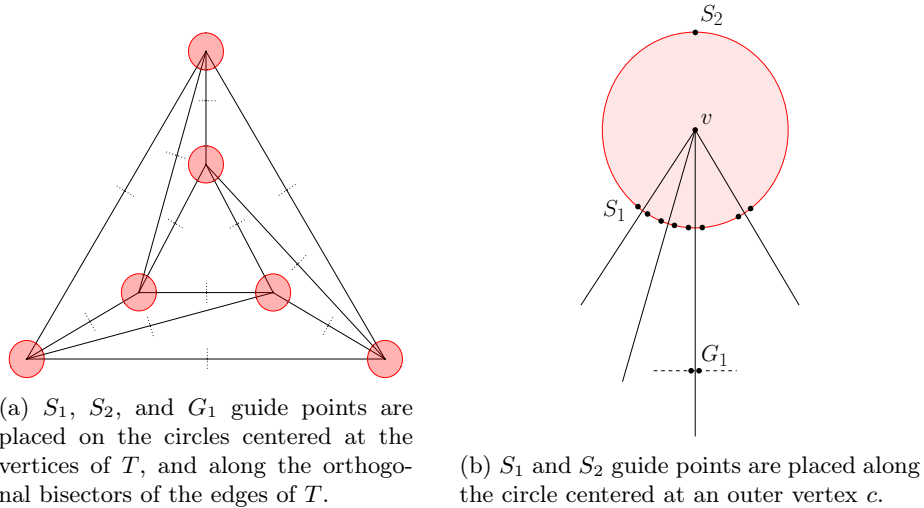


Fig. 3: Guide points placed in Stage 1.

Stage 2. We place parabolic arcs through the guide points placed in Stage 1 as follows: For each edge e of T , we place two parabolic arcs, one on each side of e , that contain all guide points associated with e : The axis of symmetry of both parabolic arcs is the orthogonal bisector of e ; the endpoints of each arc are S_1 guide points, and its midpoint is a G_1 guide point.

For each vertex v of T , connect all pairs of consecutive guide points along the circle centered at v by line segments. These segments determine a convex polygon, called a *vertex gadget*, inscribed in the circle.

In every triangular face Δ of T , the three parabolic arcs and three line segments between pairs of parabolic arcs form a closed curve $\gamma(\Delta)$. We claim that the interior of $\gamma(\Delta)$ is a convex region if $\eta > 0$ is sufficiently small. It is enough to show that $\gamma(\Delta)$ is convex in the neighborhood of every S_1 guide point. Consider a parabolic arc associated with an edge e of Δ . As $\eta \rightarrow 0$, this arc converges to a line segment parallel to e , connecting two S_1 guide points. Furthermore, the directions of the tangent lines of the arc at the two S_1 guide points converge to the direction of e . In the limit, we have $\eta = 0$ and $\gamma(\Delta)$ is a convex hexagon. Consequently, $\gamma(\Delta)$ is already convex for all sufficiently small values of $\eta > 0$ in the neighborhood of every S_1 guide point. We can now state the last condition on η : Let $\eta > 0$ be sufficiently small such that (3) the interior of $\gamma(\Delta)$ is convex for every triangular face Δ of T .

Similarly, for each edge $e = v_i v_j$ of the outer face of T , we also create a convex region, which is bounded by a parabolic arc associated with e in the outer face, the two line segments between S_1 and S_2 guide points in the circles centered at v_i and v_j , and by rays emanating from the S_2 guide points to infinity. Specifically, at each S_2 guide point, we extend one of the two incident segments between S_1 and S_2 guide points into a ray. The result of these modifications are illustrated in Fig. 4.

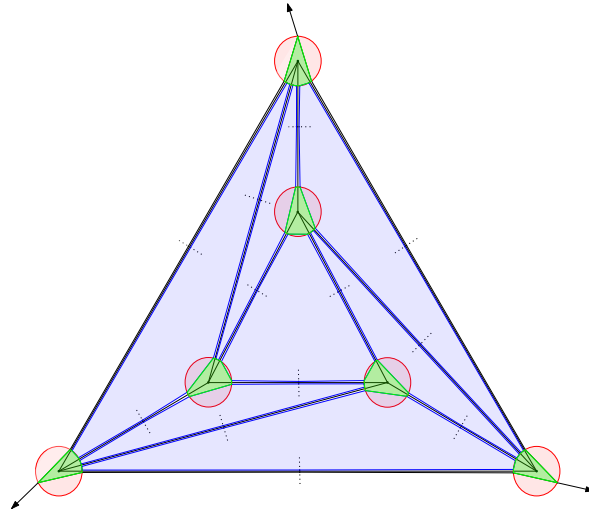


Fig. 4: The convex regions in blue are the modified faces of T , and convex polygons centered at the inner and outer vertices of T are in green.

Stage 3. In the previous stage, we created convex regions in the interior of the faces of T (one in each triangular face, and three in the outer face), but these regions do not cover any of the edges of e . In this stage, we place a convex polygon (called a *subface*) in each of these previously created region, and subdivide the complement of the subfaces into convex polygons (called *edge gadgets* and *vertex gadgets*), using additional guide points.

Consider an edge $e = v_i v_j$ of T . By a suitable rotation, we may assume that e lies on the x -axis, the orthogonal bisector of e is on the y -axis, and $x(v_i) < 0 < x(v_j)$. In Stage 2, we created two parabolic arcs, one on each side of e , such that their endpoints are S_1 guide points on the circles centered at v_i and v_j , resp., and their middle points are G_1 guide points on the y -axis. Along each parabolic arc, we place four additional guide points with x -coordinates $\pm \frac{1}{6} |v_i v_j|$ and $\pm \frac{1}{3} |v_i v_j|$, resp., and call them S_3 *guide points*. As a result, there are seven guide points on each parabola in the pattern $S_1, S_3, S_3, G_1, S_3, S_3,$ and S_1 ; see Fig. 5.

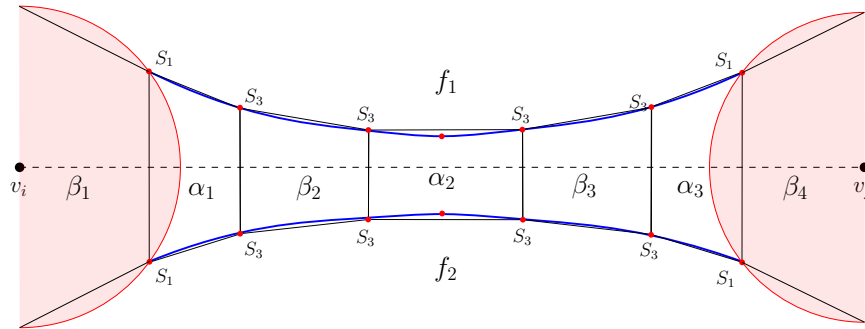


Fig. 5: Additional guide points placed along the edges of a subface, and parabolic arcs are shown in blue.

We connect every pair of S_1 or S_3 guide points that have the same x -coordinate, on opposite sides of e , by a line segment. In each parabolic arc, we also connect consecutive S_1 or S_3 guide points by line segments; see Fig. 5. Note that we do not connect the two G_1 points. Five trapezoids are formed by these line segments, and we call them *edge gadgets*. Furthermore, we distinguish between two types of edge gadgets: Alternately α - and β -gadgets along the edge (i.e., three α -gadgets and two β -gadgets).

We also classify vertex gadgets, created in Stage 2, as β -gadgets. Consequently, each edge of T is covered by seven gadgets: Alternately β - and α -gadgets along the edge (i.e., three α -gadgets and four β -gadgets); see Fig. 6.

By connecting the S_1 and S_3 guide points in each parabolic arc, we create a polygonal path. In each convex region defined in Stage 2, we replace the parabolic arc by this polygonal path, and obtain a convex polygon, called a *subface*.

Note that the subfaces, vertex gadgets, and edge gadgets jointly form a convex subdivision of the entire plane.

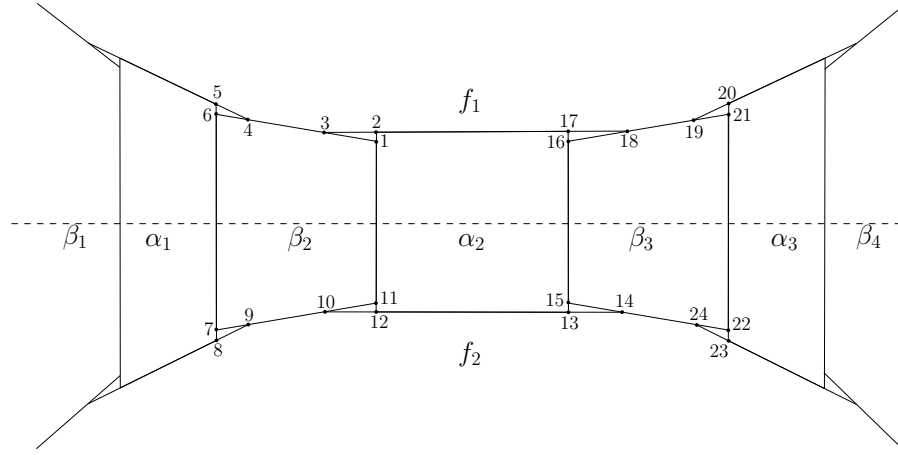


Fig. 6: For a pair of subfaces, the gadgets alternate between β - and α -gadgets.

Stage 4. In the final stage of our construction, we modify the edges of the edge gadgets created in the previous stage to create a planar occlusion diagram. We translate or extend some of the edges by a sufficiently small distance δ , $0 < \delta < \eta/2$. For each pair of adjacent subfaces and β -gadgets, we perform the following modifications. Translate the line segment s on the boundary between the two faces by distance $\delta > 0$ towards the interior of the β -gadget, and extend the two adjacent edges of the subface until they hit (the translated segment) s ; as shown in Fig. 6. Each such perturbation creates two swirls, each of which is adjacent to a subface, an α -gadget and a β -gadget.

As a result, each segment is blocked by another segment at each endpoint, and all segments that hit the same segment reach it from the same side. The perturbations in Stage 4 ensure these property for all segments on the boundaries of α - and β -gadgets; and it also holds for the three rays extending to infinity by construction. By Definition 2, these segments form a POD.

4 Nonrealizability of Planar Occlusion Diagrams

Suppose, for contradiction, that the POD \mathcal{S} constructed in Section 3 is realizable for every $\varepsilon > 0$. First we deduce useful properties for any realization \mathcal{P} for a fixed ε . We then consider the limit of the realizations as ε goes to zero: The subfaces converge to the triangles of the triangulation T (in Fig. 2), and we show that the realizations of the subfaces converge to the upper envelop of a convex polyhedron, contradicting the nonrealizability of T (Theorem 1).

Properties of a realization \mathcal{P} for a fixed $\varepsilon > 0$. For a face f in the POD \mathcal{S} , we denote by \hat{f} the polygon in the lower envelope of \mathcal{P} such that f is the orthogonal projection of \hat{f} ; we call \hat{f} the *realization* of f . (Note that \hat{f} is contained in some polygon $F \in \mathcal{P}$, but the vertices of F are not in the lower envelope of \mathcal{P} , consequently \hat{f} is a proper subset of F .)

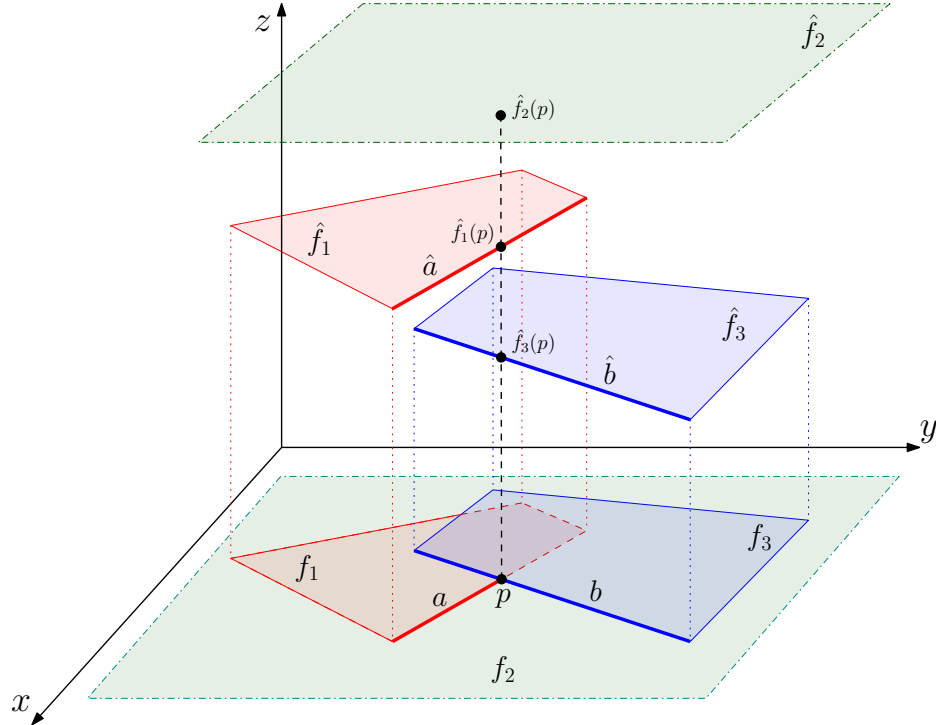


Fig. 7: A point p incident to faces f_1 , f_2 , and f_3 of a POD. It is the projection of the points \hat{f}_1 , \hat{f}_2 , and \hat{f}_3 in a realization in 3-space.

Let $a, b \in \mathcal{S}$ such that a hits b at point p ; refer to Fig. 7. Then p is incident to three faces of the POD, say f_1 , f_2 and f_3 such that f_1 and f_2 are on opposite sides of a , and f_3 is incident to b . Then p is the orthogonal projection of three points, that we denote by $\hat{f}_i(p) \in \hat{f}_i$ for $i \in \{1, 2, 3\}$. Since $\hat{f}_3(p)$ occludes both $\hat{f}_1(p)$ and $\hat{f}_2(p)$ from the viewpoint $z = -\infty$, then $\hat{f}_3(p)$ lies below $\hat{f}_1(p)$ and $\hat{f}_2(p)$, or equivalently $z(\hat{f}_3(p)) \leq z(\hat{f}_1(p))$ and $z(\hat{f}_3(p)) \leq z(\hat{f}_2(p))$. For example, at vertex 1 in Figs. 6–8, the point $\hat{\beta}_2(1)$ in the polygon $\hat{\beta}_2$ is occluded by the point $\hat{\alpha}_2(1)$ in the polygon $\hat{\gamma}_2$. Similarly at vertex 3, the point $\hat{\beta}_2(3)$ occludes the point $\hat{f}_1(3)$.

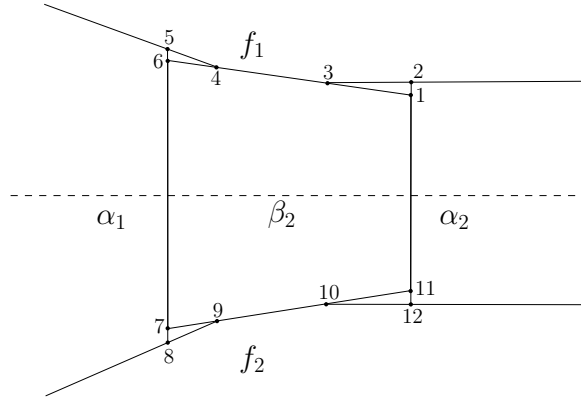


Fig. 8: Labelled vertices of the planar occlusion diagram

In the following lemmas, we analyze the relation between (the realizations of) two subfaces corresponding to two adjacent triangles of T . Let f_1 and f_2 be subfaces lying in two adjacent triangles of T .

Lemma 3. *Consider a β -edge gadget adjacent to both subfaces f_1 and f_2 , as depicted in Fig. 8. Then $\hat{f}_2(8)$ or $\hat{f}_2(12)$ is below the plane $\text{span}(\hat{f}_1)$.*

Proof. Notice $\hat{\beta}_2(4)$ and $\hat{\beta}_2(3)$ are below $\text{span}(\hat{f}_1)$. Then at least one of $\hat{\beta}_2(1)$ and $\hat{\beta}_2(6)$ is also below $\text{span}(\hat{f}_1)$, because all points on the line segment $\hat{\beta}_2(1)\hat{\beta}_2(6)$ are collinear, and the z -coordinates monotonically decrease from one end to the other. Assume first that $\hat{\beta}_2(1)$ is below $\text{span}(\hat{f}_1)$. Then $\hat{\alpha}_2(1)$ is below $\text{span}(\hat{f}_1)$ since $\hat{\alpha}_2(1)$ is below $\hat{\beta}_2(1)$. Since $\hat{f}_1(2)$ is below $\hat{\alpha}_2(2)$, then the z -coordinate monotonically decrease along the line segment $\hat{\alpha}_2(2)\hat{\alpha}_2(12)$, and so $\hat{\alpha}_2(12)$ is also below $\text{span}(\hat{f}_1)$. Finally, since $\hat{f}_2(12)$ is below $\hat{\alpha}_2(12)$, then $\hat{f}_2(12)$ is below $\text{span}(\hat{f}_1)$. If, however, $\hat{\beta}_2(6)$ is below $\text{span}(\hat{f}_1)$, then a symmetric argument shows that $\hat{f}_2(8)$ is below $\text{span}(\hat{f}_1)$. \square

By Lemma 3, \hat{f}_1 contains a point below $\text{span}(\hat{f}_2)$, and symmetrically \hat{f}_2 contains a point below $\text{span}(\hat{f}_1)$. Denote by $\hat{d}_1 \in \hat{f}_1$ and $\hat{d}_3 \in \hat{f}_2$ the points below $\text{span}(\hat{f}_2)$ obtained from the β -gadget β_2 ; and by $\hat{d}_2 \in \hat{f}_1$ and $\hat{d}_4 \in \hat{f}_2$ the points below $\text{span}(\hat{f}_1)$ obtained from β_3 . Let d_1, \dots, d_4 , resp., be the orthogonal projections of $\hat{d}_1, \dots, \hat{d}_4$ to the xy -plane; see Fig. 9. Note that the points d_1, \dots, d_4 are S_3 guide points created in Stage 3 of the construction.

Lemma 4. *The planes $\text{span}(\hat{f}_1)$ and $\text{span}(\hat{f}_2)$ are not parallel.*

Proof. Lemma 3 shows that point $\hat{d}_1 \in \hat{f}_1$ lies below $\text{span}(\hat{f}_1)$, and point $\hat{d}_3 \in \hat{f}_2$ lies below $\text{span}(\hat{f}_2)$. It follows that the planes $\text{span}(\hat{f}_1)$ and $\text{span}(\hat{f}_2)$ are distinct, and neither plane lies entirely above the other. Consequently, $\text{span}(\hat{f}_1)$ and $\text{span}(\hat{f}_2)$ are not parallel. \square

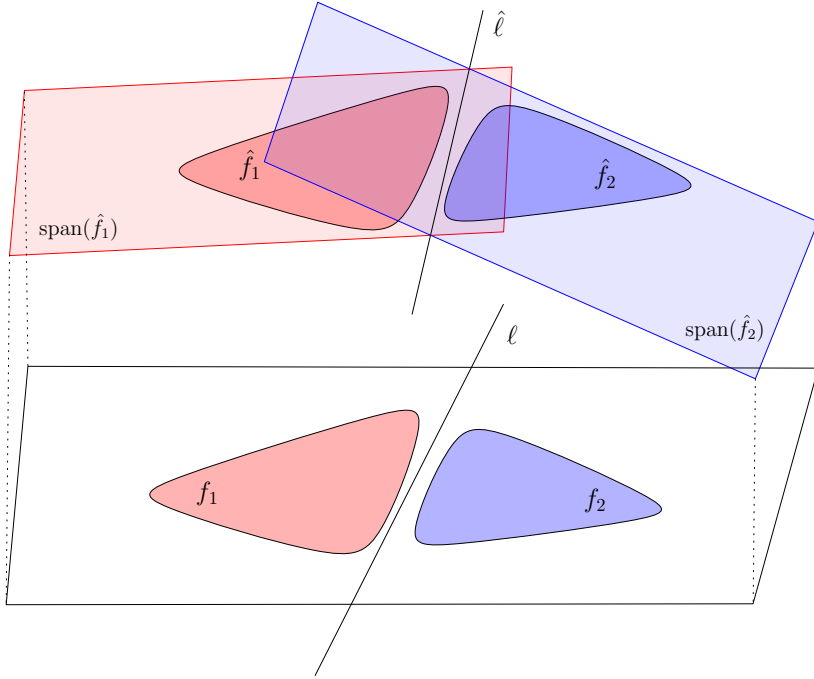


Fig. 9: Subfaces f_1 and f_2 in the xy -plane, and their realizations \hat{f}_1 and \hat{f}_2 in \mathbb{R}^3 . Line $\hat{\ell} = \text{span}(\hat{f}_1) \cap \text{span}(\hat{f}_2)$, and its orthogonal projection ℓ .

As $\text{span}(\hat{f}_1)$ and $\text{span}(\hat{f}_2)$ are nonparallel, by Lemma 4, their intersection is a line that we denote by $\hat{\ell} = \text{span}(\hat{f}_1) \cap \text{span}(\hat{f}_2)$. Let ℓ be the orthogonal projection of $\hat{\ell}$ onto the xy -plane. Note that ℓ may intersect the interior of f_1 or f_2 ; see Fig. 10 for an example. Let H_1 be the halfplane in the plane $\text{span}(\hat{f}_1)$ bounded by the line $\hat{\ell}$ that contains the center of \hat{f}_1 , and similarly, let H_2 be the halfplane in $\text{span}(\hat{f}_2)$ bounded by the line $\hat{\ell}$ that contains the center of \hat{f}_2 .

Lemma 5. *The dihedral angle between H_1 and H_2 is convex from below.*

Proof. Since $\hat{d}_1, \hat{d}_2 \in \hat{f}_1$ are below $\text{span}(\hat{f}_2)$ and $\hat{d}_3, \hat{d}_4 \in \hat{f}_2$ are below $\text{span}(\hat{f}_1)$ in \mathbb{R}^3 , then the points $d_1, d_2 \in f_1$ and $d_3, d_4 \in f_2$ are on opposite sides of the line ℓ in the xy -plane.

By construction, the center of f_1 (resp., f_2) is on the same side of ℓ as the points $d_1, d_2 \in f_1$ (resp., points $d_3, d_4 \in f_2$). By Lemma 3, H_1 lies below $\text{span}(\hat{f}_2)$ and H_2 lies below $\text{span}(\hat{f}_1)$, which implies that the dihedral angle between H_1 and H_2 is convex from below, as claimed. \square

The limit of realizations as ε goes to zero. In the remainder of this section, we consider a sequence of PODs \mathcal{S} as $\varepsilon \rightarrow 0$. Note that the POD \mathcal{S} and the line ℓ depend on ε , but the triangulation T does not. Let v_i and v_j denote the two

common vertices of the triangles in T that contain the subfaces f_1 and f_2 ; and let $L = \text{span}(v_i v_j)$ be the line spanned by the edge $v_i v_j$.

Lemma 6. *The line ℓ converges to L as $\varepsilon \rightarrow 0$.*

Proof. By a suitable rotation, we may assume that $v_i v_j$ lies on the x -axis, the orthogonal bisector of $v_i v_j$ is the y -axis, $x(v_i) < 0 < x(v_j)$, and furthermore, f_1 and f_2 lie above and below the x -axis, respectively. Since the points d_1, \dots, d_4 are S_3 guide points, which lie on two parabolas constructed in Stage 2, then the absolute values of the x and y -coordinates of these points are bounded by

$$\frac{1}{6} |v_i v_j| \leq |x(d_i)| < \frac{1}{3} |v_i v_j| \quad (1)$$

and

$$0 < \frac{\eta}{2} < |y(d_i)| < \eta \leq \frac{\varepsilon}{2} \quad (2)$$

for all $i \in \{1, \dots, 4\}$; see Fig. 10. Using (1) and (2), the absolute value of the

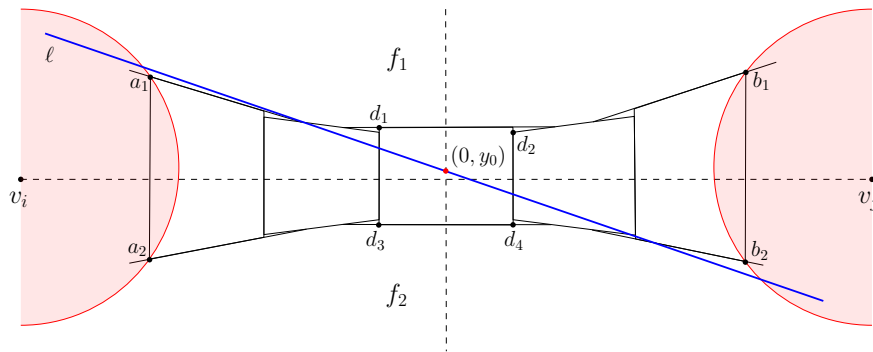


Fig. 10: A possible location for the line ℓ in blue, that separates points $d_1, d_2 \in f_1$ and $d_3, d_4 \in f_2$.

slope of ℓ is bounded by

$$0 \leq \text{slope}(\ell) \leq \left| \max\{\text{slope}(d_2 d_3), \text{slope}(d_1 d_4)\} \right| < \frac{2\eta}{\frac{2}{3} |v_i v_j|} < \frac{3\varepsilon}{2 |v_i v_j|}.$$

This shows that $\lim_{\varepsilon \rightarrow 0} \text{slope}(\ell) = 0$.

Let y_0 be the y -intercept of line ℓ (i.e., $(0, y_0)$ is the intersection point of ℓ with the y -axis); see Fig. 10. Since the line segments $d_1 d_2$ and $d_3 d_4$ are above and below ℓ , resp., and both $d_1 d_2$ and $d_3 d_4$ cross the y -axis, then y_0 lies between the y -intercepts of $d_1 d_2$ and $d_3 d_4$. Now (2) yields

$$-\frac{\varepsilon}{2} < \min\{y(d_3), y(d_4)\} \leq y_0 \leq \max\{y(d_1), y(d_2)\} < \frac{\varepsilon}{2}.$$

In particular, this implies $\lim_{\varepsilon \rightarrow 0} y_0 = 0$. \square

We are now ready to prove our main results on planar occlusion diagrams.

Theorem 1. *There exists a POD that is not realizable.*

Proof. Suppose, for contradiction, that every POD is realizable. For every $n \in \mathbb{N}$, let \mathcal{S}_n be the POD constructed above with $\varepsilon = \frac{1}{n}$, and let \mathcal{P}_n be its realization (that is, \mathcal{S}_n is the orthogonal projection of the lower envelope of \mathcal{P}_n). Let $H_n \in \mathcal{P}_n$ denote the face that corresponds to the subspace in the central triangle in T ; and let $U_n \subset \mathbb{R}^3$ denote the set of all points in \mathcal{P}_n that orthogonally project to segment endpoints in \mathcal{S}_n . By Lemma 4, the polygons in \mathcal{P}_n are not all coplanar. We may assume, by a suitable affine transformation, that H_n lies in the xy -plane, the z -coordinates of all point in U_n are in the interval $[-1, 1]$ and the z -coordinate of at least one point in U_n is in $\{-1, 1\}$ for all $n \in \mathbb{N}$.

By compactness, there exists a subsequence $(n_k)_{k=1}^\infty$ such that the point set U_{n_k} converges as $k \rightarrow \infty$. Note that the realization of each subspace in \mathcal{P}_{n_k} is determined by U_{n_k} . Let \mathcal{F} denote the set of subspaces in the limit; and let $\mathcal{Q} = \text{conv}(\mathcal{F})$ be the convex hull of all points in \mathcal{Q} .

Consider two subspaces, f_1 and f_2 , that correspond to adjacent triangles in T . In the limit, \hat{f}_1 and \hat{f}_2 are adjacent triangles in \mathbb{R}^3 , and by Lemma 5 their dihedral angle (from below) is at most π (they might be coplanar). That is, the triangles in \mathcal{F} form the upper envelope of \mathcal{Q} , where each facet of \mathcal{Q} is the union of one or more triangles in \mathcal{F} . In particular, T is a triangulation of the orthogonal projection of the upper envelope of \mathcal{Q} onto the xy -plane. By assumption, one facet of the upper envelope lies in the xy -plane and another facet contains a point with nonzero z -coordinate. This implies that the upper envelope of \mathcal{Q} consists of two or more facets, but a triangulation of its orthogonal projection onto the xy -plane is the triangulation T in Fig. 2, contradicting Lemma 2. \square

5 Nonrealizability of Spherical Occlusion Diagrams

We are now ready to prove our main result.

Theorem 2. *There exists an SOD that is not realizable.*

Proof. By Theorem 1, there exists a nonrealizable POD \mathcal{S} , which is a POD constructed in Section 3 for a sufficiently small $\varepsilon > 0$. We construct a SOD \mathcal{D} as follows. Let R be a sufficiently large equilateral triangle that contains all segment endpoints of \mathcal{P} .

Let \mathcal{D}_0 be an SOD depicted in Fig. 1. It is the visibility map of six disjoint axis-aligned rectangles along the facets of a cube in \mathbb{R}^3 . Note that \mathcal{D}_0 contains eight triangular swirls. We may assume, by symmetry, that all swirls are equilateral (spherical) triangles. Let R_0 be one of the swirls of \mathcal{D}_0 .

There exists a suitable spherical projection ϱ that maps R to R_0 . Indeed, assume that \mathcal{P} lies in the plane $H : z = -1$ in \mathbb{R}^3 , the barycenter of the triangle R is $(0, 0, -1) \in H$, and the (spherical) barycenter of R_0 is also $(0, 0, -1) \in \mathbb{S}^2$. Then the stereographic projection of H to \mathbb{S}^2 maps R to an equilateral (spherical) triangle in \mathbb{S}^2 . A suitable scaling followed by this stereographic projection ensures

that R is mapped to R_0 . Now ϱ maps the segments of \mathcal{S} within R into a set \mathcal{D}_1 of geodesic arcs in \mathcal{R}_0 . Now $\mathcal{D} = \mathcal{D}_0 \cup \mathcal{D}_1$ is an SOD \mathcal{D} .

We claim that \mathcal{D} is not realizable. Suppose, for contradiction, that $\mathcal{D} = \mathcal{P}_s$ for a polygonal scene \mathcal{P} and a viewpoint $s \in \mathbb{R}^3$. Let $\mathcal{Q} \subset \mathcal{P}$ be the subset of polygons that correspond to the arcs in \mathcal{D}_1 . A projective transformation that maps s to $z = -\infty$ will also map \mathcal{Q} to a polygonal scene \mathcal{Q}' . Now \mathcal{Q}' realizes the POD \mathcal{S} , contradicting the choice of \mathcal{S} . \square

By modifying the construction above, we also prove Viglietta's conjecture [10, Conjecture 5] about irreducible SODs.

Theorem 3. *There exists an irreducible SOD that is not realizable.*

Proof. In Section 3, we have constructed a nonrealizable POD \mathcal{S} . By construction, \mathcal{S} has rotational symmetry through angle $\frac{2\pi}{3}$ around the origin, and contains precisely three rays, which are contained in three nonconcurrent lines. Let \mathcal{S}' be the image of \mathcal{S} reflected in a line. We construct an SOD \mathcal{D} as follows. Let \mathcal{D}_0 be an SOD depicted in Fig. 1, that consists of 12 arcs, forming 4 clockwise and 4 counterclockwise swirls, and has reflection symmetry in all three coordinate planes. Use spherical projections to map a copy of \mathcal{S} to each clockwise swirl, and a copy of \mathcal{S}' to each counterclockwise swirl, such that the three rays in each copy of a POD are mapped to the three arcs of the swirl. We obtain an SOD \mathcal{D} .

We claim that \mathcal{D} is irreducible and nonrealizable. Suppose, for contradiction, that $\mathcal{D} = \mathcal{P}_s$ for a polygonal scene \mathcal{P} and a viewpoint $s \in \mathbb{R}^3$. Let $\mathcal{Q} \subset \mathcal{P}$ be the subset of polygons that correspond to the arcs in one copy of \mathcal{S} . A projective transformation that maps s to $z = -\infty$ will also map \mathcal{Q} to a polygonal scene \mathcal{Q}' . Now \mathcal{Q}' realizes the POD \mathcal{S} , contradicting the choice of \mathcal{S} . \square

6 Conclusions

We have shown that spherical occlusion diagrams (SODs) are not equivalent to visibility maps in 3-space. Our result raises several open problems: Is there a simple (axiomatic) characterization of visibility maps? Can one decide efficiently whether a given SOD is a visibility map? If so, can one find a realization efficiently? What is the maximum (combinatorial, topological, or bit) complexity of the realization space for an SOD with n arcs for a given positive integer n ?

References

1. Basu, S., Dhandapani, R., Pollack, R.: On the realizable weaving patterns of polynomial curves in \mathbb{R}^3 . In: Proc. 12th Sympos. Graph Drawing (GD). LNCS, vol. 3383, pp. 36–42. Springer (2004). https://doi.org/10.1007/978-3-540-31843-9_5
2. Cano, J., Tóth, C.D., Urrutia, J., Viglietta, G.: Edge guards for polyhedra in three-space. *Comput. Geom.* **104**, 101859 (2022). <https://doi.org/10.1016/j.comgeo.2022.101859>

3. De Loera, J.A., Rambau, J., Santos, F.: Regular triangulations and secondary polytopes. In: *Triangulations: Structures for Algorithms and Applications*, pp. 209–274. Springer, Berlin (2010). https://doi.org/10.1007/978-3-642-12971-1_5
4. Lee, C.W., Santos, F.: *Subdivisions and triangulations of polytopes*, chap. 16. CRC Press, Boca Raton, FL, 3rd edn. (2017)
5. O’Rourke, J.: *Art Gallery Theorems and Algorithms*. Oxford University Press (1987)
6. O’Rourke, J.: *Visibility*, chap. 33. CRC Press, Boca Raton, FL, 3rd edn. (2017)
7. Pach, J., Pollack, R., Welzl, E.: Weaving patterns of lines and line segments in space. *Algorithmica* **9**(6), 561–571 (1993). <https://doi.org/10.1007/BF01190155>
8. Tóth, C.D., Urrutia, J., Viglietta, G.: Minimizing visible edges in polyhedra. In: *Proceedings of the 23rd Thailand-Japan Conference on Discrete and Computational Geometry Graphs, and Games (TJCDCGGG)*. pp. 70–71 (2021)
9. Viglietta, G.: A theory of spherical diagrams. Preprint (2021). <https://doi.org/10.48550/arXiv.2107.05895>
10. Viglietta, G.: A theory of spherical diagrams. *Computing in Geometry and Topology* **2**(2), 2:1–2:24 (2023). <https://doi.org/10.57717/cgt.v2i2.30>